Available online at www.sciencedirect.com
SCIENCE DIRECT®
Journal of Organometallic Chemistry 690 (2005) 1570–1580
Journal of Organometallic Chemistry
www.elsevier.com/locate/jorganchem

Nickel (II) complexes bearing 2-ethylcarboxylate-6-iminopyridyl ligands: synthesis, structures and their catalytic behavior for ethylene oligomerization and polymerization

Xiubo Tang [a], Wen-Hua Sun [a,*], Tielong Gao [a], Junxian Hou [a], Jiutong Chen [b], Wei Chen [c]

[a] Key Laboratory of Engineering Plastics, Institute of Chemistry, Chinese Academy of Sciences, Beijing 100080, China
[b] State Key Laboratory of Structural Chemistry, Fujian Institute of Research on the Structure of Matter, Chinese Academy of Sciences, Fuzhou 350002, China
[c] National Polyolefin Engineering and Research Center, Beijing Research Institute of Chemical Industry, China Petroleum & Chemical Corporation, Beijing 100013, China

Received 7 October 2004; revised 9 December 2004; accepted 21 December 2004
Available online 12 January 2005

Abstract

A series of nickel (II) complexes (L)$NiCl_2$ (**7**–**9**) and (L)$NiBr_2$ (**10**–**12**) were prepared by the reactions of the corresponding 2-carboxylate-6-iminopyridine ligands **1**–**6** with $NiCl_2 \cdot 6H_2O$ or (DME)$NiBr_2$ (DME = 1,2-dimethoxyethane), respectively. All the complexes were characterized by IR spectroscopy and elemental analysis. Solid-state structures of **7**, **8**, **10**, **11** and **12** were determined by X-ray diffraction. In the cases of **7**, **8** and **10**, the ligands chelate with the nickel centers in tridentate fashion in which the carbonyl oxygen atoms coordinate with the metal centers, while the carbonyl oxygen atoms are free from coordinating with the nickel centers in **11** and **12**. Upon activation with methylaluminoxane (MAO), these complexes are active for ethylene oligomerization (up to 7.97×10^5 g mol^{-1} (Ni) h^{-1} for **11** with 2 equivalents of PPh_3 as auxiliary ligand) and/or polymerization (1.37×10^4 g mol^{-1} (Ni) h^{-1} for **9**). The ethylene oligomerization activities of **7**–**12** were significantly improved in the presence of PPh_3 as auxiliary ligands. The effects of the coordination environment and reaction conditions on the ethylene catalytic behaviors have been discussed.

Keywords: Iminopyridine ligand; Nickel complexes; Ethylene oligomerization; Polymerization

1. Introduction

The oligomerization of ethylene as the major industrial process provides linear α-olefins, which are extensively used as comonomer of polyolefin, surfactants and lubricants. The linear α-olefins were originally manufactured by the Ziegler (Alfen) process [1], and current industrial catalysts include either alkylaluminum compound or a combination of alkylaluminum compound with early transition metal compounds or nickel (II) with bidentate monoanionic [P,O] ligands (the SHOP process) [2]. Various nickel complexes containing chelating ligands such as diimine [N,N] [3], salicylaldimine [N,O] [4], pyridylimine [N,N] [5], and [P,N] [6] ligands serve as highly active catalysts for ethylene oligomerization or polymerization. The coordination environments of these well-defined catalysts can be systematically varied by changing the substituents in the ligand

* Corresponding author. Tel.: +86 10 62557955; fax: +86 10 62618239.
E-mail address: whsun@iccas.ac.cn (W.-H. Sun).

0022-328X/$ - see front matter © 2005 Elsevier B.V. All rights reserved.
doi:10.1016/j.jorganchem.2004.12.027

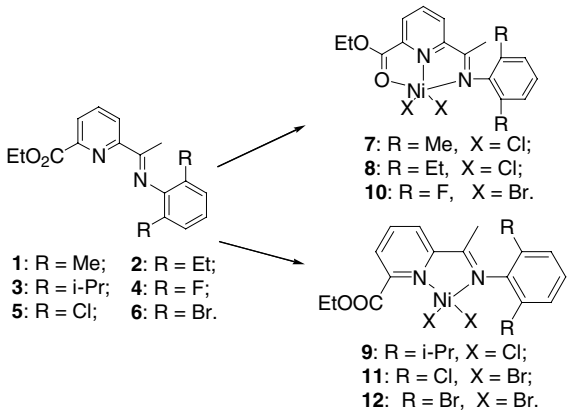

Scheme 1. The synthesis of the complexes **7**–**12**.

backbones, which provides an opportunity to control their ethylene catalytic behaviors, including the activities and the product distributions. In addition, the late-metal catalysts have the advantages such as less oxophilicity and the tolerance of expanded functional groups, which might open a door to copolymerization of ethylene and polar monomers [7]. Recently, we reported a new family of iron (II) and cobalt (II) complexes bearing carboxylate ester-substituted iminopyridine ligands, which were verified to perform well as the catalysts for ethylene oligomerization and polymerization upon activation with methylaluminoxane (MAO), and α-olefins are the resultant products [8]. We extended the research with same ligands into nickel complexes. Owning to the bonding versatility of the carboxylate substituent in the ligands, the coordination fashions of these nickel complexes are different in solid state. In the presence of MAO as cocatalyst, the Ni (II) complexes showed the favorable ethylene oligomerization versus polymerization. The selectivity for α-olefins by nickel complexes is relative lower than its ferrous analogues, and the resultant polyethylene is branched. The substituents in the ligand backbones of the complexes are systemically varied from the electron-donating alky groups to electron-withdrawing halogen group, which provide an insight into both electric and steric effects on their ethylene oligomerization and polymerization performance. The ethylene oligomerization activities increase by one order of magnitude when additional PPh_3 is employed as auxiliary ligand.

2. Results and discussion

2.1. Synthesis of pyridylimine nickel (II) complexes

The ester-substituted pyridylimine ligands **1**–**6** [2-CO_2Et-6-(2,6-$R_2C_6H_3N{=}CCH_3$)C_5H_3N (**1**: R = CH_3, **2**: R = Et, **3**: R = i-Pr, **4**: R = F, **5**: R = Cl, **6**: R = Br)] were prepared with the previously reported procedures [8]. The dichloride nickel complexes **7**–**9** were obtained by stirring the ethanol solution of $NiCl_2 \cdot 6H_2O$ with the ligands **1**–**3** at room temperature, while the dibromide complexes **10**–**12** were prepared by the reaction of (DME)$NiBr_2$ (DME = 1,2-dimethoxyethane) with the corresponding ligands **4**–**6** (Scheme 1). These complexes were characterized by IR spectroscopic and elemental analysis. The paramagnetic nature of the nickel complexes precludes the NMR characterization. These complexes show high stability in both its solution and solid state. The IR spectra of the ligands show that the C=N stretching frequencies appear in the range of 1640–1655 cm^{-1} [8], while the C=N stretching vibrations shift toward lower frequencies between 1619 and 1625 cm^{-1} with weak intensities for complexes **9**–**12**. The results indicate the coordination interaction between the imino nitrogen atom and the nickel center. Moreover, the C=O stretching vibrations in IR spectra show slight red shift by ca. 10–20 cm^{-1} for the nickel complexes.

2.2. Solid-state structures of the pyridylimine nickel (II) complexes

It is notable that these complexes display different colors in solid state. Complexes **7**, **8** and **10** are bright yellow, while **9**, **11** and **12** are red brown, which suggests that these complexes might adopt different coordination fashions. The single crystal X-ray diffraction determination provides direct evidences of the individual structures, and fortunately the single crystals of **7**, **8**, **10**, **11** and **12** suitable for X-ray diffraction were obtained. Selected bond lengths and bond angles for complexes **7**, **8**, **10** and **11**, **12** are listed in Tables 1 and 2, and their crystallographic data and refinement are given in Table 3. Crystals of **7** were grown from its ethanol solution layering with diethyl ether. As shown in Fig. 1, the coordination geometry around the nickel center of **7** is a pseudo-square-pyramid. The ester-substituted pyridylimine ligand coordinates with the nickel center as a tridentate ligand through nitrogen atoms of imine and pyridine as well as carbonyl oxygen atom. The plane of the dimethyl-substituted aryl ring is essentially oriented orthogonally to the coordination plane (85.1°).

Crystals of **8** were grown from a dichloromethane solution layering with pentane, and its molecular structure is shown in Fig. 2. The carbonyl oxygen atom O1 also coordinates with the nickel center, therefore the ligand chelates in N∧N∧O tridentate fashion. The geometry around the nickel atom can be described as a distorted octahedron, with an adventitious water molecule incorporating into the coordination sphere during the crystal growth. The Ni–N (pyridyl) bond distance (Ni–N1, 2.005 (3) Å) is about 0.12 Å shorter than the

Table 1
Selected bond lengths and bond angles for complex **7**, **8** and **10**

Complex **7**		Complex **8**		Complex **10**	
Bond lengths (Å)					
Ni(1)–N(1)	2.006(4)	Ni(1)–N(1)	2.005(3)	Ni–N(1)	2.016(4)
Ni(1)–N(2)	2.094(4)	Ni(1)–N(2)	2.122(3)	Ni–N(2)	2.100(4)
Ni(1)–Cl(1)	2.2133(18)	Ni(1)–Cl(1)	2.3618(12)	Ni–Br(1)	2.4854(8)
Ni(1)–Cl(2)	2.272(2)	Ni(1)–Cl(2)	2.3096(12)	Ni–Br(2)	2.5013(9)
N(2)–C(6)	1.285(6)	N(2)–C(6)	1.281(5)	N(2)–C(9)	1.287(7)
Ni(1)–O(1)	2.402(5)	Ni(1)–O(1)	2.342(3)	Ni–O(1)	2.409(4)
Ni(1)···O(2)	4.280	Ni(1)···O(2)	4.284	Ni···O(2)	4.346
		Ni(1)–O(3)	2.178(3)	Ni–O(3)	2.147(4)
Bond angles (°)					
N(1)–Ni(1)–N(2)	77.89(15)	N(1)–Ni(1)–N(2)	78.06(12)	N(1)–Ni–N(2)	77.99(16)
N(1)–Ni(1)–O(1)	73.89(16)	N(1)–Ni(1)–O(1)	74.60(10)	N(1)–Ni–O(1)	73.65(15)
N(2)–Ni(1)–O(1)	149.66(17)	N(2)–Ni(1)–O(1)	152.30(10)	N(2)–Ni–O(1)	150.80(15)
N(1)–Ni(1)–Cl(1)	146.84(17)	N(1)–Ni(1)–O(3)	85.68(11)	N(1)–Ni–O(3)	88.19(17)
N(2)–Ni(1)–Cl(1)	103.38(11)	N(2)–Ni(1)–O(3)	92.60(12)	N(2)–Ni–O(3)	89.88(15)
N(1)–Ni(1)–Cl(2)	93.19(13)	N(1)–Ni(1)–Cl(1)	88.33(8)	N(1)–Ni–Br(1)	174.78(13)
N(2)–Ni(1)–Cl(2)	103.27(15)	N(1)–Ni(1)–Cl(2)	171.77(9)	N(1)–Ni–Br(2)	88.99(13)
Cl(1)–Ni(1)–O(1)	94.37(13)	N(2)–Ni(1)–Cl(1)	98.15(9)	N(2)–Ni–Br(1)	103.83(12)
Cl(2)–Ni(1)–O(1)	89.35(16)	N(2)–Ni(1)–Cl(2)	104.16(9)	N(2)–Ni–Br(2)	96.10(12)
Cl(1)–Ni(1)–Cl(2)	118.04(8)	O(1)–Ni(1)–O(3)	81.11(11)	O(1)–Ni–O(3)	82.51(14)
		O(1)–Ni(1)–Cl(1)	85.47(7)	O(1)–Ni–Br(1)	103.85(9)
		O(1)–Ni(1)–Cl(2)	102.33(7)	O(1)–Ni–Br(2)	90.25(10)
		O(3)–Ni(1)–Cl(1)	166.34(9)	O(3)–Ni–Br(1)	86.92(11)
		O(3)–Ni(1)–Cl(2)	86.30(8)	O(3)–Ni–Br(2)	172.72(10)
		Cl(1)–Ni(1)–Cl(2)	99.11(4)	Br(1)–Ni–Br(2)	95.64(3)

Table 2
Selected bond lengths and bond angles for complex **11** and **12**

Complex **11**		Complex **12**	
Bond lengths (Å)			
Ni–N(1)	2.061(6)	Ni(1)–N(1)	1.974(6)
Ni–N(2)	2.078(6)	Ni(1)–N(2)	2.087(6)
Ni–Br(1)	2.4990(11)	Ni(1)–Br(1)	2.3672(15)
Ni–Br(2)	2.4656(12)	Ni(1)–Br(2)	2.3296(15)
N(2)–C(6)	1.302(9)	N(2)–C(7)	1.275(9)
Ni–O	2.096(6)	Ni(1)···O(1)	2.436
Ni···O(1)	2.559	Ni(1)···O(2)	4.330
Ni···O(2)	4.458		
Bond angles (°)			
N(1)–Ni–N(2)	78.7(2)	N(1)–Ni(1)–N(2)	78.8(2)
N(1)–Ni–Br(1)	174.96(17)	N(1)–Ni(1)–Br(1)	108.65(17)
N(2)–Ni–Br(1)	101.58(17)	N(2)–Ni(1)–Br(1)	104.19(18)
N(1)–Ni–Br(2)	89.63(17)	N(1)–Ni(1)–Br(2)	125.13(18)
N(2)–Ni–Br(2)	99.83(17)	N(2)–Ni(1)–Br(2)	104.47(17)
Br(1)–Ni–Br(2)	95.25(4)	Br(1)–Ni(1)–Br(2)	122.56(5)
N(1)–Ni–O	88.2(2)		
N(2)–Ni–O	97.4(2)		
O–Ni–Br(1)	86.78(15)		
O–Ni–Br(2)	161.90(16)		

Ni–N (imino) bond distance (Ni–N2, 2.122(3) Å). The plane of the phenyl ring is oriented approximately orthogonal to the coordination plane with the angle of 82.5°. Deviation of the nickel center from the plane formed by the coordinated N1, N2 and O1 is 0.038 Å. Crystals of **10** were grown from a dichloromethane solution layering with hexane. The molecular structure is depicted in Fig. 3. The coordination geometry around nickel center of **10** is similar to that of **8**, despite two bromo atoms, instead of chloro atoms, coordinating with the central nickel, as well as the presence of the fluoro atoms instead of the ethyl groups in the *ortho*

Table 3
Crystallographic data and refinement for **7**, **8**, **10**, **11** and **12**

	7	**8**	**10**	**11**	**12**
Formula	$C_{18}H_{20}Cl_2N_2NiO_2$	$C_{20}H_{27}Cl_2N_2NiO_{3.5}$	$C_{16}H_{16}Br_2F_2N_2NiO_3$	$C_{16}H_{16}Br_2Cl_2N_2NiO_3$	$C_{16}H_{14}Br_4N_2NiO_2 \cdot CH_2Cl_2$
Formula weight	425.97	481.05	540.84	573.74	729.57
Crystal system	Orthorhombic	Triclinic	Monoclinic	Monoclinic	Triclinic
Space group	*Pca2*(1)	$P\bar{1}$	*C2/c*	*C2/c*	$P\bar{1}$
a (Å)	13.706(3)	7.997(3)	25.4776(6)	27.79620(10)	8.0963(16)
b (Å)	9.866(2)	9.907(3)	10.2440(3)	10.3562(3)	9.1394(18)
c (Å)	14.247(3)	14.630(5)	15.575	19.1319(3)	16.844(3)
α (°)	90	92.516(6)	90	90	103.70(3)
β (°)	90	97.226(5)	90.7610(10)	133.1160(10)	97.17(3)
γ (°)	90	101.403(5)	90	90	94.46(3)
V (Å^3)	1926.5(7)	1124.3(7)	4044.32(15)	4020.22(13)	1194.0(4)
Z	4	2	8	8	2
D_{calcd} (g cm^{-3})	1.469	1.421	1.766	1.896	2.209
Abs coefficient, μ (mm^{-1})	1.298	1.125	4.964	5.225	7.744
F(0 0 0)	880	502	2128	2256	700
θ range (°)	2.06–27.48	1.21–26.47	1.61–24.92	2.01–25.06	2.31–27.48
Number of data collected	2284	6477	6312	5736	5149
Number of unique data	2284	4548	3495	3488	2900
R (%)	0.0436	0.0514	0.0442	0.0561	0.0732
R_w (%)	0.1122	0.1259	0.1028	0.1229	0.1698
Goodness of fit	1.065	1.076	1.193	1.162	0.985

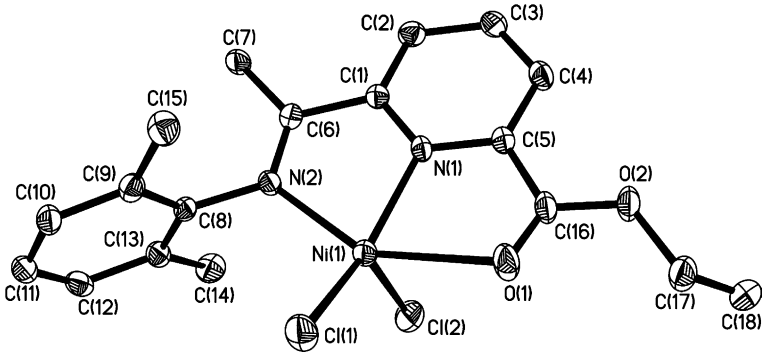

Fig. 1. The molecular structure of **7**. Hydrogen atoms are omitted for clarity.

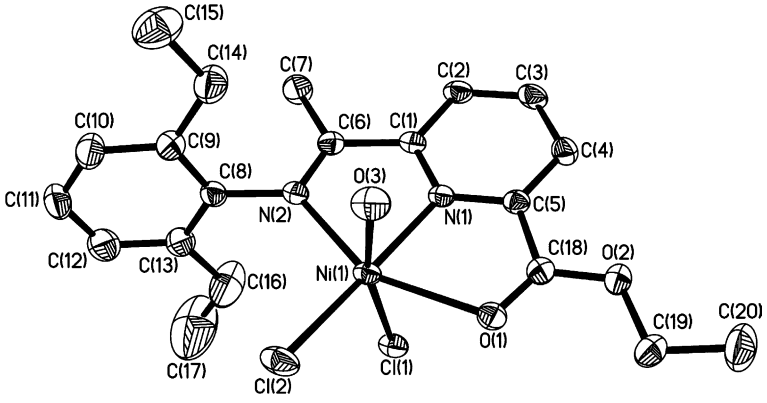

Fig. 2. The molecular structure of **8**. Hydrogen atoms are omitted for clarity.

positions of the phenyl ring. It is notified that the Ni–O1 bonding lengths of **7** (2.402 Å), **8** (2.342(3) Å) and **10** (2.409(4) Å) are longer than the previously reported Ni–O bond length values [9], which indicates the weak interactions between nickel and carbonyl oxygen.

Crystals of **11** were grown through diffusing hexane layer into its dichloromethane solution. X-ray structure

determination indicates that the carbonyl oxygen atom O2 deviates away from the central nickel instead of coordinating and the distance between Ni and O2 is 4.458 Å. One adventitious water molecule incorporates into the coordination sphere. The geometry of the five-coordinated nickel complex **11** can be better described as distorted square pyramidal with the four atoms N1, O, Br1 and Br2 forming the bottom plane and the N2 atom occupying the apical position (Fig. 4). The dichlorophenyl ring lies almost perpendicular to the coordination plane (80.1°). It should be pointed out that the water molecule is involving into the complexes in **8, 10** and **11** during the crystal growth, and the powders used for ethylene catalytic reaction might have no water.

Crystals of **12** were grown through diffusing hexane layer into its dichloromethane solution, and the molecular structure is shown in Fig. 5. X-ray structure characterization conforms that the complex **12** adopts the N∧N coordination fashion. One dichloromethane molecule is included in the crystal lattice without binding interaction with the complex. The geometry around the metal center can be described as a distorted tetrahedron. The dibromophenyl ring lies nearly perpendicular to the coordination plane (the dihedral angle is 92.0°). The distance between the nickel atom and carbonyl oxygen O1 (2.436 Å) in **12** is slightly longer than the Ni–O(1) bond lengths in **7**, **8** and **10**, indicative of the presence of weaker interaction between the carbonyl oxygen and the nickel atom. The coordination geometry around the nickel center of **7**–**12** was affected by the backbones of their ligand, however, there is no unambiguous explanation yet.

2.3. Ethylene oligomerization and polymerization

The catalytic activities of precatalysts **7**–**12** for ethylene oligomerization and polymerization have been carried out in the presence of methylaluminoxane (MAO) as cocatalyst. In all cases, these catalysts generate butenes and hexenes as main oligomeric product and the distribution of oligomers does not follow Schulz–Flory rules. No odd carbon number oligomers were detected in the GC and GC/MS analysis. For the bulky substituted catalysts, small amount of polyethylene is also produced.

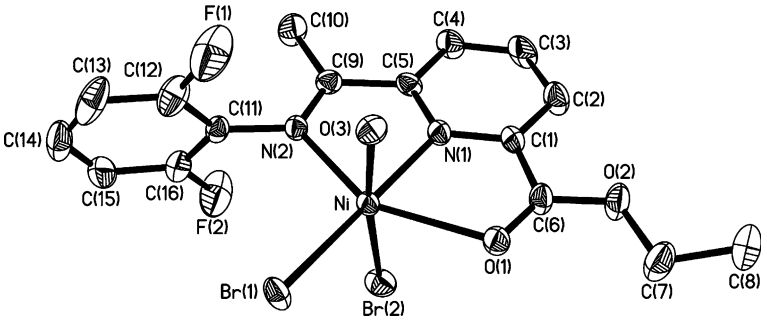

Fig. 3. The molecular structure of **10**. Hydrogen atoms are omitted for clarity.

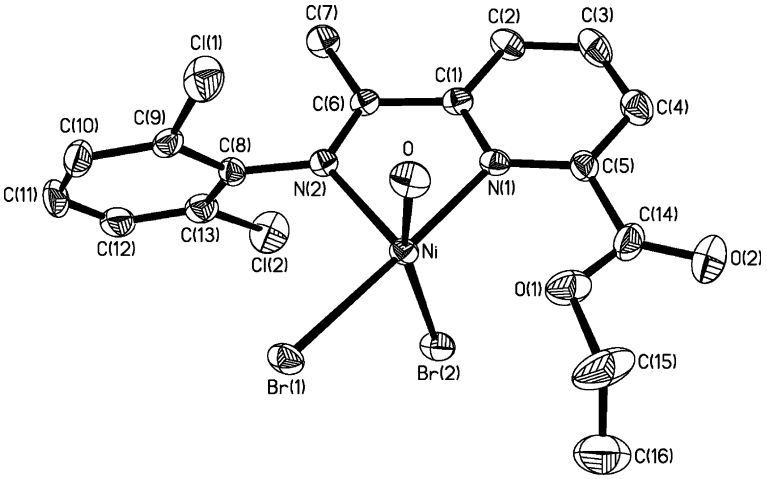

Fig. 4. The molecular structure of **11**. Hydrogen atoms are omitted for clarity.

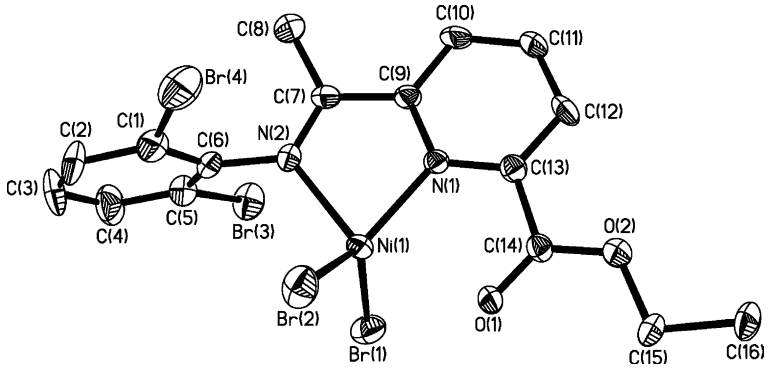

Fig. 5. The molecular structure of **12**. Hydrogen atoms and solvent molecule (CH_2Cl_2) are omitted for clarity.

2.3.1. Effects of ligands environment

The results of ethylene oligomerization and polymerization with the nickel complexes as precatalysts at 1 atm are collected in Table 4. It can be observed that the ligand environment has considerable effects on their catalytic behaviors, such as activity and product distribution. The complex **9** with bulky diisopropyl-substituted ligand produces oligomers with higher order carbon number olefins ($C_{\geqslant 8}$ over 40%) and more polyethylene than **7** and **8** under the identical reaction conditions (entry 3 vs entry 1 and 2, Table 4). Similarly, for complexes **10**–**12** with halogen substituents in the ligand backbone, the dibromo-substituted **12** generates polyethylene in low activity, while the less bulky substituted **10** and **11** produce only oligomers (entry 6 vs entry 4 and 5 in Table 4). These observations are well consistent with the established rules that the bulky substitutes in the *ortho*-positions will provide efficient steric blocking in the axial sites and retard the β-hydrogen elimination. Thus, the higher carbon number oligomers are favorable for the precatalysts with bulkier substituents [a]. The effect of the substituents in the ligands on the ethylene oligomerization activities is not so definite as its on the product distribution (entry 1–6 in Table 4).

It is worth noting that complex **10** containing the difluoro-substituted ligand shows the lowest activity under the identical reaction conditions, which may be attributed to the readily deactivation of the active species formed from **10** due to the small size of the difluoro substituents. Similar result was obtained in our recent study on ethylene catalytic activities for the ferrous and cobaltous bearing pyridylimine ligands [8]. Gibson has shown that the catalytic intermediates formed from precursors containing pyridyldiimine ligands lacking sufficient steric bulk in the *ortho*-aryl positions are more easily deactivated through an interaction with alkylaluminum reagent [10].

Table 4
Results of ethylene oligomerization and polymerization with **7**–**12**/MAO at 1 atm[a]

Entry	Precatalyst	Al/Ni	Temperature (°C)	Time (min)	Oligom distribution[b] (%)				Activity 10^4 g mol^{-1} (Ni) h^{-1}	
					$C_4/\Sigma C$	$C_6/\Sigma C$	$C_{\geqslant 8}/\Sigma C$	Linear α-olefin	Oligom[b]	Polym
1	**7**	1000	15	30	80.63	5.19	14.17	8.9	8.88	0.308
2	**8**	1000	15	30	77.30	5.67	17.02	14.7	9.17	trace
3	**9**	1000	15	30	48.53	8.73	42.74	7.9	5.47	1.37
4	**10**	1000	15	30	87.86	1.66	10.48	40.4	4.08	no
5	**11**	1000	15	30	84.28	10.25	5.47	11.1	12.10	no
6	**12**	1000	15	30	70.15	21.89	7.96	51.0	9.04	0.30
7	**12**	500	15	30	87.76	2.50	9.74	21.5	8.71	0.42
8	**12**	1500	15	30	66.85	7.61	25.54	26.1	8.96	0.20
9	**12**	2000	15	30	80.50	5.37	14.13	28.6	5.52	trace
10	**12**	1000	0	30	75.00	7.15	17.85	33.0	7.81	0.74
11	**12**	1000	40	30	71.24	19.76	9.00	49.1	21.30	0.26
12	**12**	1000	60	30	73.67	3.17	23.16	53.1	2.30	trace
13[c]	**12**	1000	15	60	84.35	12.15	3.50	6.4	12.40	0.168

[a] General conditions: 5 μmol precatalyst, 30 ml toluene as solvent.
[b] Determined by GC. ΣC denotes the total amounts of oligomers.
[c] Determined by GC–MS.

2.3.2. Effects of reaction parameter

To probe the effects of reaction parameters on the ethylene oligomerization and polymerization behaviors, the catalyst precursor **12** was typically investigated *via* changing the amounts of MAO, the reaction temperature and the reaction time.

The oligomerization activity values show slight frustration when the Al/Ni molar ratio is varied in the range of 1000–1500. Further increase the Al/Ni ratio to 2000 leads to noticeable decrease in oligomerization activity. The decrease in the oligomerization activity with excessive MAO might be caused by the impurities such as alkyl aluminum in commercial MAO, which will lead to the deactivation of the active catalytic sites. In addition, the polymerization activities remarkably decease with the increase of the Al/Ni molar ratio. The correlation between the polymer productivity and the Al/Ni molar ratio suggests that the chain transfer to aluminum might occur in the polymerization cases. Reaction temperature remarkably affects the oligomerization activity, and the highest oligomerization activity is observed at the temperature of 40 °C. The precatalyst might not be fully activated at lower temperature. Further elevating the reaction temperature (60 °C) leads to sharp reduction in oligomerization activities (Table 4, entry 12), which may be ascribed to the decomposition of the active catalytic sites and lower ethylene solubility at higher temperature. In addition, the PE productivity decreases with the increase of the reaction temperature, which suggests the increase of the rate of chain transfer relative to the rate of chain propagation at the higher temperature. Higher oligomerization activity is observed for 60 min versus 30 min (Table 4, entry 6 vs 13), which indicates the existence of induction period of the catalyst.

It should be pointed out that the selectivities for linear α-olefins of oligomers are varied with the ligand environments and reaction parameters, however, no unambiguous trend can be summarized according to the values obtained. In general, the selectivities for α-olefins are relative low. For example, as determined by GC–MS for the oligomers obtained in entry 13 in Table 4, C4 fraction contains 1-butene (minor) and 2-butene (major) while C6 fraction contains 1-hexene (minor), 2-hexene (major) and a small amount of 2-methyl-2-pentene. In general, the selectivity for linear α-olefins is lower than their iron analogues [8]. The low selectivity for linear α-olefin with the nickel complexes **7**–**12** can be attributed to their ability to reversibly eliminate β-H after ethylene insertion and reinsert the olefin with the opposite regiochemistry and give 2-butene after chain transfer or to lead to isomerization of 1-butene by a re-uptake mechanism [6i]. The ability of Ni(II) complexes to isomerizes α-olefins was also observed in previous studies [6c,6h].

2.3.3. Effects of ethylene pressure

The ethylene oligomerization and polymerization behaviors for precatalysts **9** and **12** were also investigated at 10 atm, and the results are shown in Table 5. The results show that increase of ethylene concentration has a little effect on the catalytic activities and product distributions for **9** and **12**. This is in sharp contrast with the results for their iron analogues, for which the oligomer distributions and productivities are significantly impacted by the increase of the ethylene pressure [8]. GPC analysis reveals that the molecular weight of the PE produced by **9** and **12** is relative low with the M_n value of 5500 and 2000, respectively. As shown by the GPC traces in Fig. 6, the PE samples display bimodal (PE produced by **9**) or trimodal (PE produced by **12**) behaviors, which might be attributed to the formation of different type of active species after activated by MAO and the difference of the rate of chain transfer relative to chain propagation of these active species. With literatures explained, chain transfer to aluminum also might result in broad multimodal distribution of the PE [7b,7c]. The corresponding DSC curves show multimodality as well. The PE sample produced by **9** at 10 atm was selected for ^{1}H and ^{13}C NMR characterization. Less useful information on the microstructure of the PE is obtained from the ^{1}H NMR spectrum because of the resonance overlap. The ^{13}C NMR analysis (Fig. 7) reveals that the PE sample contains small amount of *n*-butyl branches.

Table 5
Results of ethylene oligomerization and polymerization with **9** and **12** at 10 atm[a]

Entry	Precatalyst (μmol)	Polym yield (g)	Activity, 10^4 g mol^{-1} (Ni) h^{-1}		M_n[c] (×10^3)	Linear α-olefin (%)[b]	PDI[c]	T_m[d] (°C)
			Oligom[b]	Polym				
1	**9** (56.0)	0.85	4.88	1.50	5.5	15.9	63.2	128
2	**12** (43.8)	0.18	27.10	0.40	2.0	29.5	25.4	123

[a] General conditions: Al/Ni = 1000, 15 °C, 1 h, 700 ml toluene.
[b] Determined by GC.
[c] Determined by GPC.
[d] Determined by DSC.

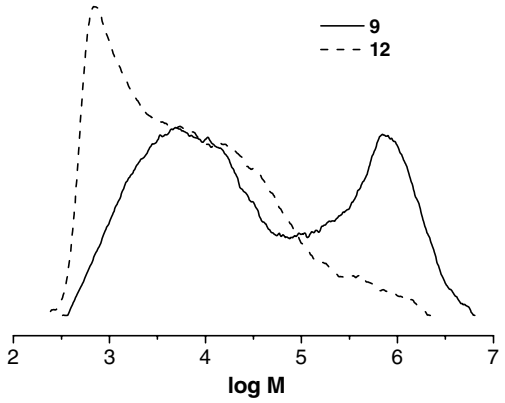

Fig. 6. GPC traces of the PE samples generated by **9** and **12** at 10 atm.

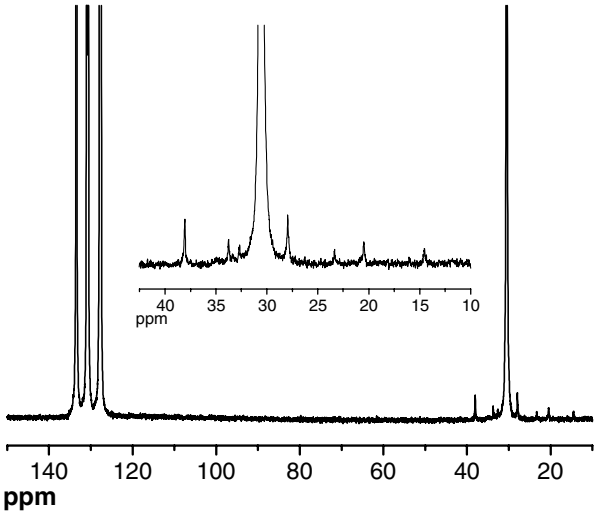

Fig. 7. ^{13}C NMR spectra of the polyethylene sample generated by **9** in entry 1, Table 4.

The branching degree is about 2*n*-butyls per 1000 methylenes in the main chain. Assignments of the ^{13}C NMR chemical shifts and calculation of the branching degree were performed according to the previously reported methods [11].

2.3.4. Effects of auxiliary ligand (PPh_3)

For catalyst precursors **9**–**12**, oligomerization activities were remarkably enhanced when PPh_3 was used as the auxiliary ligand, and the results are summarized in Table 6. Similar effect of PPh_3 was observed in the previous reports [12]. Contrarily, the decrease of ethylene polymerization activity was also reported due to the addition of 5 equiv of PPh_3 for the neutral nickel (II) catalyst [13]. GC analysis indicates that the presence of PPh_3 in the reaction system affects the oligomer distributions as well. Low-order carbon number oligomers are produced without polyethylene due to the incorporation of PPh_3 in the reaction system. Variation of auxiliary ligand amount affects the oligomerization activities of the catalyst precursor **12**, and 2 equiv of PPh_3 is optimal (Table 6, entries 6, 7 and 8). The turnover number (TON) keeps increasing when the reaction time is increased from 30 to 90 min (13,000, 24,000 and 25,000 for 30, 60 and 90 min, respectively), although the activity value decreases, which indicates that the active catalytic species are still alive after 60 min.

The mechanism of the acceleration phenomena of ethylene oligomerzation induced by the addition of the auxiliary ligand PPh_3 is not well disclosed. We tentatively attributed it to the temporary coordination of PPh_3 with the vacant site formed by the action of MAO, thus the active catalytic species are protected. Remarkable induction period was observed during the oligomerization reaction in the presence of PPh_3, which might reflect the coordination of PPh_3 with the vacant site. The PPh_3 group may dissociate again upon approach and coordination of ethylene monomer. Further studies to understand the effects of the auxiliary ligand on the ethylene oligomerization are in progress.

Table 6
Ethylene oligomerization with **7**–**12**/MAO in presence of PPh_3 at 1 atm[a]

Entry	Precatalyst	Al/Ni/PPh_3	Time (min)	Oligom distribution (%)[b]			Activity[b] 10^5 g mol^{-1} (Ni) h^{-1}
				$C_4/\Sigma C$	$C_6/\Sigma C$	Linear α-olefin	
1	**7**	1000:1:2	30	86.00	12.98	9.7	6.66
2	**8**	1000:1:2	30	76.35	21.86	9.3	6.50
3	**9**	1000:1:2	30	76.49	21.62	8.8	6.52
4	**10**	1000:1:2	30	86.10	13.90	7.9	5.83
5	**11**	1000:1:2	30	98.12	0.47	9.8	7.97
6	**12**	1000:1:1	30	84.78	14.56	10.6	4.91
7	**12**	1000:1:2	30	81.68	17.09	8.7	7.92
8	**12**	1000:1:4	30	81.62	17.50	7.9	5.10
9	**12**	1000:1:2	60	78.39	21.48	2.2	6.69
10	**12**	1000:1:2	90	76.74	23.15	2.0	4.46

[a] General conditions: 5 μmol of precatalyst, 30 ml toluene as solvent, temp: 15 °C.
[b] Determined by GC. ΣC denotes the total amounts of oligomers.

3. Conclusion

A series of nickel complexes containing 2-carboxylate-6-iminopyridine ligands were synthesized. X-ray determination reveals that these complexes adopt different coordination fashions. Upon activation with MAO, these complexes show considerable to high catalytic activities for ethylene oligomerization with C_4–C_8 olefins as the main products. Complexes **7**, **8**, **9** and **12** with bulky substituents in the *ortho*-positions of the aryl ring in the ligand backbone display low ethylene polymerization activities simultaneously. Addition of PPh_3 as auxiliary ligand leads to higher catalytic activity.

4. Experimental

4.1. General considerations

All manipulations of air- and/or moisture-sensitive were performed under nitrogen atmosphere using standard Schlenk techniques. Solvents were dried by the literature methods. Methylaluminoxane (MAO) was purchased from Albemarle as a 1.4 M solution in toluene. Other reagents were purchased from Aldrich or Acros Chemicals. IR spectra were recorded on a Perkin–Elmer system 2000 FT-IR spectrometer. Elemental analysis was carried out using HP-MOD 1106 microanalyzer. GC analysis was performed with a Carlo Erba Strumentazione gas chromatograph equipped a flame ionization detector and a 30 m (0.25 mm i.d., 0.25 μm film thickness) DM-1 silica capillary column. GC–MS analysis was performed with HP 5890 SERIES II and HP 5971 SERIES mass detector. The yield of oligomer was calculated by referencing with the mass of the used solvent based on the prerequisite that the mass of each fraction is approximately proportional to its integrated areas in the GC trace. Selectivity for linear α-olefin is defined as: (amounts of linear α-olefin of all fractions/total amounts of oligomer products)%. ^1H and ^{13}C NMR spectra of the PE samples were recorded on Bruker DMX-400 MHz instrument at 135 °C in 1,2-dichlorobenzene-d_4 using TMS as internal standard. Molecular weight and polydispersity index (PDI) of PE was determined by a PL-GPC220 at 150 °C with 1,2,4-trichlorobenzene as an eluent. Melting points of the polymers were obtained on a Perkin–Elmer DSC-7 in the standard DSC run mode. The instrument was initially calibrated for melting point of an indium standard at a heating rate of 10 °C/min. The polymer sample was first equilibrated at 0 °C and then heated to 160 °C at a heating rate of 10 °C/min to remove the heat history. The sample was then cooled to 0 °C at a rate of 10 °C/min. A second heating cycle was used for collected DSC thermo gram data at a ramping rate of 10 °C/min.

4.2. Synthesis of (L)$NiCl_2$ (**7–9**; L = **1–3**)

7–9 were prepared by similar method, thus, only the synthesis of **7** is detailed described. To ligand **1** (0.286 g, 1 mmol) and $NiCl_2 \cdot H_2O$ (0.237 g, 1 mmol), was added fresh distilled ethanol (5 ml) at the room temperature. The solution turned to orange immediately. After stirred for 10 h, hexane (20 ml) was added to precipitate the complex. After filtrated and washed with hexane, the product was dried in vacuo. The desired complex was obtained as bright yellow powder in 90.0% yield. IR (KBr): 1695 ($\nu_{C=O}$); 1624 ($\nu_{C=N}$); 1592; 1469; 1375 cm^{-1}. Anal. Calc. for $C_{18}H_{20}Cl_2N_2NiO_2$: C, 50.75; H, 4.73; N, 6.58. Found: C, 50.48; H, 4.81; N, 6.46%. **8** was obtained as bright yellow powder in 92.3% yield. IR (KBr): 1689 ($\nu_{C=O}$); 1621 ($\nu_{C=N}$); 1590; 1467; 1377 cm^{-1}. Anal. Calc. for $C_{20}H_{24}Cl_2N_2NiO_2$: C, 52.91; H, 5.33; N, 6.17. Found: C, 52.89; H, 5.35; N, 5.90%. **9** was obtained as red brown powder in 89.0% yield. IR (KBr): 1694 ($\nu_{C=O}$); 1619 ($\nu_{C=N}$); 1591; 1445; 1376 cm^{-1}. Anal. Calc. for $C_{22}H_{28}Cl_2N_2NiO_2$: C, 54.81; H, 5.85; N, 5.81. Found: C, 54.80; H, 5.87; N, 5.70%.

4.3. Synthesis of (L)$NiBr_2$ (**10–12**; L = **4–6**)

10–12 were synthesized by the same method, thus, only the synthesis of **10** was described. Ligand **4** (0.100 g, 0.32 mmol), (DME)$NiBr_2$ (0.1159 g, 0.32 mmol) and dichloromethane (10 ml) were added to the flask at the room temperature. The solution turned to orange immediately. After stirred for 10 h, the solution was concentrated to about 4 ml, and then hexane (20 ml) was added to precipitate the complex. After filtrated and washed with hexane, the product was dried in vacuo. The desired complex was obtained as bright yellow powder in 91.1% yield. IR (KBr): 1686 ($\nu_{C=O}$); 1625 ($\nu_{C=N}$); 1592; 1473; 1375 cm^{-1}. Anal. Calc. for $C_{16}H_{14}Br_2F_2N_2NiO_2 \cdot H_2O$: C, 35.53; H, 2.98; N, 5.18. Found: C, 35.14; H, 2.93; N, 5.08%. **11** was obtained as red brown powder in 84.0% yield. IR (KBr): 1693 ($\nu_{C=O}$); 1623 ($\nu_{C=N}$); 1592; 1436; 1375 cm^{-1}. Anal. Calc. for $C_{16}H_{14}Br_2Cl_2N_2NiO_2 \cdot H_2O$: C, 33.50; H, 2.81; N, 4.88. Found: C, 33.20; H, 2.61; N, 4.62%. **12** was obtained as red brown powder in 93.0% yield. IR (KBr): 1695 ($\nu_{C=O}$); 1622 ($\nu_{C=N}$); 1592; 1429; 1374 cm^{-1}. Anal. Calc. for $C_{16}H_{14}Br_4N_2NiO_2 \cdot CH_2Cl_2$: C, 27.96; H, 2.27; Br, N, 3.84; Found: C, 28.01; H, 2.27; N, 3.82%. For complexes **10**, **11** and **12**, X-ray crystal structure determination also confirms the existence of water molecule or dichloromethane molecule.

4.4. Procedure for 1 atm ethylene oligomerization and polymerization

Precatalyst (5 μmol) was added to a fully dried Schlenk flask under nitrogen. The flask was back-filled

three times with N_2 and twice with 1 atm ethylene, and then charged with toluene and MAO solution in turn. Under prescribed temperature, the reaction solution was vigorously stirred under 1 atm ethylene for the desired period. The polymerization reaction was quenched by addition 60 ml 10% HCl solution. About 1 ml of organic solution was dried by anhydrous Na_2SO_4 for GC or GC–MS analysis. The remained mixture was poured into 100 ml of ethanol to precipitate the polymer. The ployethylene was isolated via filtration and dried at 60 °C to constant weight in a vacuum oven.

4.5. Procedure for 10 atm ethylene oligomerization and polymerization

High-pressure ethylene polymerization was performed in a stainless steel autoclave (2 l capacity) equipped with gas ballast through a solenoid clave for continuous feeding of ethylene at constant pressure. 700 ml toluene containing the catalyst precursor was transferred to the fully dried reactor under nitrogen atmosphere. Then the required amount of cocatalyst (MAO) was injected into the reactor using a syringe. As the prescribed temperature was reached, the reactor was pressurized to 10 atm. After stirring for the desired reaction time, the reaction was quenched and worked up using the similar method described above for 1 atm reaction.

4.6. X-ray crystal structure determination

The single-crystal X-ray diffraction for **8** was carried out on a Bruker SMART 1000 CCD diffractometer with graphite monochromated Mo Kα radiation (λ = 0.71073 Å). Intensity data of crystal **7** and **12** were collected on a Rigaku RAXIS Rapid IP diffractometer with graphite monochromated Mo-Kα radiation (λ = 0.71073 Å). Intensity data of **10** and **11** were collected on a Siemens SMART CCD diffractometer with graphite monochromated Mo Kα radiation (λ = 0.71073 Å). Cell parameters were obtained by global refinement of the positions of all collected reflections. Intensities were corrected for Lorentz and polarization effects and empirical absorption. The structures were solved by direct methods and refined by full-matrix least-squares on F^2 Each H atom was placed in a calculated position and refined anisotropically. Structure solution and refinement were performed by direct methods using the SHELXL-97 Package. All the intensity data of the crystals were collected at 293(2) K. Crystal data and processing parameters for complexes **7**, **8**, **10**, **11** and **12** are summarized in Table 6.

5. Supplementary material

Crystallographic data of complexes **7**, **8**, **10**, **11** and **12** were deposited with the Cambridge Crystallographic Data Centre, CCDC 247174, 247173, 247175, 247172 and 247171, respectively. Copies of this information may be obtained free of charge from CCDC, 12 Union Road, Cambridge, CB2 1 EZ, UK (fax: +44-1223-336033; e-mail: deposit@ccdc.cam.ac.uk or http://www.ccd.cam.ac.uk).

Acknowledgements

We are grateful to the National Natural Science Foundation of China for financial supports under Grants No. 20272062 and 20473099 along with National 863 Project (2002AA333060). We thank Dr. Jinkui Niu for the English Language Corrections.

References

[1] D. Vogt, in: B. Cornils, W.A. Herrmann (Eds.), Applied Homogeneous with Organometallic Compounds, vol. 1, VCH, New York, 1996, pp. 245–258.
[2] (a) W. Keim, F.H. Kowaldt, R. Goddard, C. Kruger, Angew. Chem. Int. Ed. Engl. 17 (1978) 466;
(b) M. Peuckert, W. Keim, Organometallics 2 (1983) 594;
(c) W. Keim, A. Behr, B. Limbacker, C. Kruger, Angew. Chem. Int. Ed. Engl. 22 (1983) 503;
(d) W. Keim, A. Behr, G. Kraus, J. Organomet. Chem. 251 (1983) 377;
(e) M. Peuckert, W. Keim, J. Mol. Catal. 22 (1984) 289;
(f) W. Keim, R.P. Schulz, J. Mol. Catal. 92 (1994) 21;
(g) W. Keim, B. Hoffmann, R. Lodewick, M. Peuckert, G. Schmitt, J. Fleischhauer, U. Meier, J. Mol. Catal. 6 (1979) 79;
(h) U. Klabunde, S.D. Itten, J. Mol. Catal. 41 (1987) 123;
(i) P. Grenouillet, D. Neibecker, I. Tkatchenko, J. Organomet. Chem. 243 (1983) 213.
[3] (a) L.K. Johnson, C.M. Killian, M. Brookhart, J. Am. Chem. Soc. 117 (1995) 6414;
(b) L.K. Johnson, S. Mecking, M. Brookhart, J. Am. Chem. Soc. 118 (1996) 267;
(c) C.M. Killian, D.J. Tempel, L.K. Johnson, M. Brookhart, J. Am. Chem. Soc. 118 (1996) 11664;
(d) J. Feldman, S.J. McLain, A. Parthasarathy, W.J. Marshall, J.C. Calabrese, S.D. Arthur, Organometallics 16 (1997) 1514;
(e) M. Helldörfer, J. Backhaus, W. Milius, H.G. Alt, J. Mol. Catal. A 193 (2003) 59;
(f) D.H Camacho, E.V. Salo, J.W. Ziller, Z. Guan, Angew. Chem. Int. Ed. 43 (2004) 1821;
(g) B.Y. Lee, G.C. Bazan, J. Vela, Z.J.A. Komon, X. Bu, J. Am. Chem. Soc. 123 (2001) 5352.
[4] (a) C. Wang, S. Friedrich, T.R. Younkin, R.T. Li, R.H. Grubbs, D.A. Bansleben, M.W. Day, Organometallics 17 (1998) 3149;
(b) T.R. Younkin, E.F. Connor, J.I. Henderson, S.K. Friedrich, R.H. Grubbs, D.A. Bansleben, Science 287 (2000) 460;
(c) E.F. Connor, T.R. Younkin, J.I. Henderson, A.W. Waltman, R.H. Grubbs, Chem. Commun. (2003) 2272;
(d) L. Wang, W.-H. Sun, L. Han, Z. Li, Y. Hu, C. He, C. Yan, J. Organomet. Chem. 650 (2002) 59.
[5] (a) S.P. Meneghetti, P.J. Lutz, J. Kress, Organometallics 18 (1999) 2734;
(b) T.V. Laine, K. Lappalainen, J. Liimatta, E. Aitola, B. Loefgren, M. Leskelae, Macromol. Rapid Commun. 20 (1999) 487;

(c) T.V. Laine, U. Piironen, K. Lappalainen, M. Klinga, E. Aitola, M. Leskel, J. Organomet. Chem. 606 (2000) 112;
(d) B.Y. Lee, X. Bu, G.C. Bazan, Organometallics 20 (2001) 5425.
[6] (a) H.-P. Chen, Y.-H. Liu, S.-M. Peng, S.-T. Liu, Organometallics 22 (2003) 4893;
(b) F. Speiser, P. Braunstein, L. Saussine, R. Welter, Inorg. Chem. 43 (2004) 1649;
(c) W.-H. Sun, Z. Li, H. Hu, B. Wu, H. Yang, N. Zhu, X. Leng, H. Wang, New J. Chem. 26 (2002) 1474;
(d) P.-Y. Shi, Y.-H. Liu, S.-M. Peng, S.-T. Liu, Organometallics 21 (2002) 3203;
(e) O. Daugulis, M. Brookhart, Organometallics 21 (2002) 5926;
(f) O. Daugulis, M. Brookhart, P.S. White, Organometallics 21 (2002) 5935;
(g) F. Speiser, P. Braunstein, L. Saussine, R. Welter, Organometallics 23 (2004) 2613;
(h) F. Speiser, P. Braunstein, L. Saussine, Organometallics 23 (2004) 2625;
(i) F. Speiser, P. Braunstein, L. Saussine, Organometallics 23 (2004) 2633.
[7] (a) G.J.P. Britovsek, V.C. Gibson, D.F. Wass, Angew. Chem. Int. Ed. Engl. 38 (1999) 428;
(b) S.D. Ittel, L.K. Johnson, M. Brookhart, Chem. Rev. 100 (2000) 1169;
(c) V.C. Gibson, S.K. Spitzmesser, Chem. Rev. 103 (2003) 283.
[8] W.-H. Sun, X. Tang, T. Gao, B. Wu, W. Zhang, H. Ma, Organometallics 23 (2004) 5037.
[9] (a) F.A. Hicks, M. Brookhart, Organometallics 20 (2001) 3217;
(b) J.M. Malinoski, M. Brookhart, Organometallics 22 (2003) 5324;
(c) C.B. Shim, Y.H. Kim, B.Y. Lee, Y. Dong, H. Yun, Organometallics 22 (2003) 4272.
[10] G.J.P. Britovsek, S. Mastroianni, G.A. Solan, S.P.D. Baugh, C. Redshaw, V.C. Gibson, A.J.P. White, D. Williams, M.R.J. Elsegood, Chem. Eur. J. 6 (2000) 2221.
[11] (a) G.B. Galland, R.F. deSouza, R.S. Mauler, F.F. Nunes, Macromolecules 32 (1999) 1620;
(b) E. Kokko, P. Lehmus, R. Leino, H.J.G. Luttikhedde, P. Ekholm, J.H. Nsman, J.V. Seppälä, Macromolecule 33 (2000) 9200;
(c) G.B. Galland, R. Quijada, R. Rojas, G. Bazan, Z.J.A. Komon, Macromolecule 35 (2002) 339.
[12] (a) C. Carlini, M. Isola, V. Liuzzo, A.M.P. Galletti, G. Sbrana, Appl. Catal. A Gen. 231 (2002) 307;
(b) F.A. Hicks, J.C. Jenkins, M. Brookhart, Organometallics 22 (2003) 3533;
(c) W.-H. Sun, W. Zhang, T. Gao, X. Tang, Y. Li, X. Jin, J. Organomet. Chem. 689 (2004) 917.
[13] J.C. Jenkins, M. Brookhart, Organometallics 22 (2003) 250.